IEEE Access
Multidisciplinary | Rapid Review | Open Access Journal

Received September 9, 2016, accepted October 1, 2016, date of publication October 12, 2016, date of current version November 18, 2016.

*Digital Object Identifier 10.1109/ACCESS.2016.2616838*

# Re-Investigation of Generalized Integrator Based Filters From a First-Order-System Perspective

**ZHEN XIN[1], (Student Member, IEEE), RENDE ZHAO[2], (Member, IEEE), PAOLO MATTAVELLI[3], (Fellow, IEEE), POH CHIANG LOH[4], AND FREDE BLAABJERG[1], (Fellow, IEEE)**

[1]Department of Energy Technology, Aalborg University, Aalborg 9220, Denmark
[2]Department of Electrical Engineering, China University of Petroleum (East China), Qingdao, 266580, China
[3]Management and Engineering Department, University of Padua, Vicenza 36100, Italy
[4]Department of Electronic Engineering, The Chinese University of Hong Kong, Hong Kong, China

Corresponding author: Z. Xin (zxi@et.aau.dk)

This work was supported by European Research Council (ERC) under the European Union's Seventh Framework Program (FP7/2007-2013)/ERC Grant under Grant 321149-Harmony.

**ABSTRACT** The generalized integrator (GI)-based filters can be categorized into two types: one is related to quadrature signal generator (QSG), and the other is related to sequence filter (SF). The QSG is used for generating the in-quadrature sinusoidal signals and the SF works for extracting the symmetrical sequence components. The signals generated by QSG and SF are useful in many applications, such as grid synchronization and harmonic estimation. However, the principles of QSG and SF are usually explained by either differential equations or transfer functions, which are not appropriate for analyzing some extended structures and thus restrict their applications. To overcome the drawback, this paper uses the first-order-system concept to re-investigate the GI-based filters, with which their working principles can be intuitively understood and their structure correlations can be easily discovered. Moreover, the proposed analysis method also provides the convenience for developing improved structures. To illustrate it, two improved filters are presented to enhance the performance of the basic QSG and SF. Finally, experimental results verify the effectiveness of the proposed method.

**INDEX TERMS** Grid synchronization, signal processing, harmonic estimation, first-order system, generalized integrator, filter, quadrature-signal generator, sequence filter.

## I. INTRODUCTION

Generalized Integrator (GI), also commonly used as a resonant controller, has been widely applied for control of power converters over the past two decades. The most well-known usage is to build the Proportional-Resonant (PR) controller which is applied for current regulation in stationary frame [1]–[12]. Apart from PR controller, the other vital application is to build filters, which can be divided into two categories: one is related to Quadrature Signal Generator (QSG), and the other is related to Sequence Filter (SF).

The development timeline of the GI-based QSG (GI-QSG) can be found in Fig. 1(a), where it was initially reported in [13] and [14] for computing instantaneous active and reactive power in a single-phase system. Then, the GI-QSG was applied for grid synchronization under distorted grid voltage in [15] and [16], where it worked as a prefilter of a Phase-Locked Loop (PLL). To simplify the structure, the Second-Order-GI based Frequency-Locked Loop (SOGI-FLL) was proposed in [17], where the PLL in [15] was replaced by an FLL. Structure of the SOGI-FLL was later found to coincide with the Adaptive Notch Filter (ANF) presented in [18], while the latter was developed by Regalia [19], Bodson [20], and Hsu [21] from the fields of control engineering and signal processing. Due to the frequency-adaptive characteristic of GI-QSG, it can extract harmonics as well. Simultaneous extraction of multiple harmonics was realized by parallel GI-QSGs in [22], which was later implemented by a more explicit structure named as Multiple SOGI-FLL (MSOGI-FLL) in [23]–[25]. It should be pointed out that the same function can also be realized by ANF, whose corresponding structure has been proposed in [26]–[28]. Apart from the above applications, the GI-QSG has also been used in many other fields [29]–[35], reflecting its significance and huge potential in industrial applications.

In terms of SF, its development timeline is similar to that of GI-QSG, which is shown in Fig. 1(b). The SF was built by the sequence integrator in [11] and [12], which, unlike GI-QSG, is able to extract either positive- or

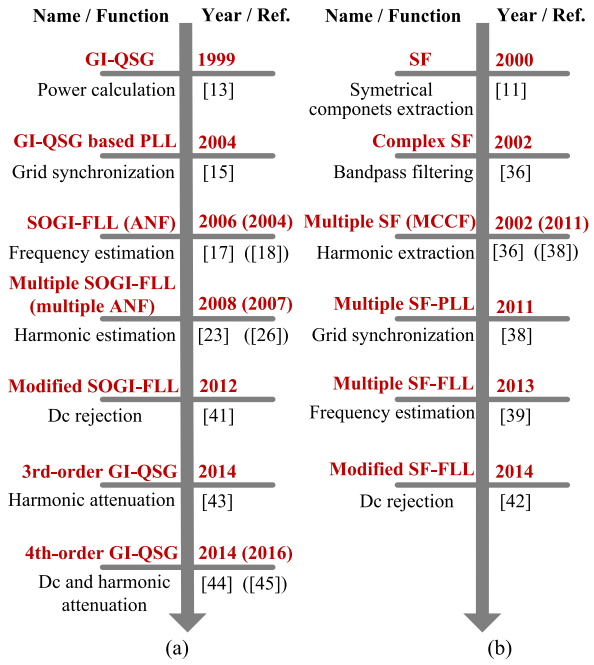


**FIGURE 1.** Development timeline of the (a) GI-QSG and (b) SF based filters.

negative-sequence component separately [11], [12]. The sequence integrator was expressed with complex transfer function in [36] and [37], whose output when fed back to its input yielded a complex band-pass filter (essentially the same with the SF in [11] and [12]) for harmonic extraction. Next, by combining multiple complex band-pass filters with a common feedback, the resulting structure enables full selectivity for all filtered harmonics [36], [37]. Again, this structure is substantially the same with the later proposed Multiple Complex-Coefficient Filter (MCCF) in [38] which was used as the prefilter of PLL. To simplify the structure, the PLL for MCCF was updated to an FLL in [39].

Unfortunately, both GI-QSG and SF produce errors when their inputs consist of dc or harmonic components. Several improved methods were thus proposed in literature, focusing on either dc-offset rejection or harmonic attenuation [40]–[44]. For instance, to remove the dc offset in the quadrature output of GI-QSG, a modified GI-QSG was reported in [41]. The same idea is then applied to SF in [42]. Besides, to enhance the high-frequency attenuation performance, the high-order GI-based filters were introduced in [43]–[45].

Despite these wide applications, structures of the above filters are dazzling and their principle illustrations are manifold and complicated, which make them difficult to be distinguished and applied properly in a short time. Traditional analysis for these filters are either based on differential equations or transfer functions, which are inconvenient to analyze some modified structures and to develop improved methods. To deal with these issues, an analysis approach from First-Order-System (FOS) perspective is proposed in this paper to re-evaluate the GI-based filters. The proposed method provides not only a generalized way to investigate the principles of GI-based filters, but also the convenience for deriving new structures. Two improved structures are proposed as examples: the first one is the Second-Order SF (SO-SF), which is superior to the SF with enhanced harmonic filtering performance; the second one is the Second-Order GI-FLL (SO-GI-FLL), which offers excellent performance under dc and/or harmonic components.

This paper is organized as follows. Section II begins by succinctly reviewing the standard FOS for dc-signal tracking. Two FOSs for sinusoidal-signal tracking are then analyzed by referring to the characteristics of the standard FOS. In Section III, several typical GI-based filters are systematically re-investigated based on the three FOSs. This is followed by Section IV, where, with the help of FOS concept, two improved GI-based structures are derived. The effectiveness of the proposed structure is finally verified through experiments in Section V, before concluding the findings in Section VI.

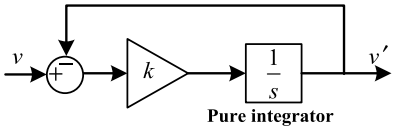


**FIGURE 2.** Block diagram of the First-Order System (FOS).

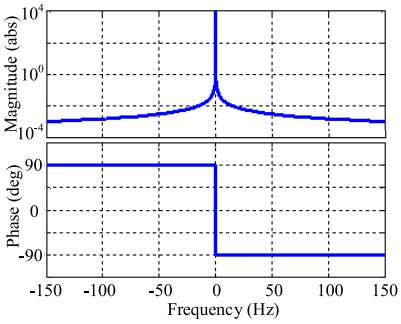


**FIGURE 3.** Magnitude/phase-frequency characteristics of the pure integrator

## II. THREE FIRST-ORDER SYSTEMS

### A. PURE INTEGRATOR AND STANDARD FIRST-ORDER SYSTEM (FOS)

The pure integrator is the core of the standard FOS shown in Fig. 2. The FOS can achieve dc-signal tracking owing to the infinite gain of the pure integrator (see Fig. 3) [46]. To illustrate their characteristics, transfer functions of the pure integrator and the FOS, and the corresponding step responses are given as

$$I(s) = \frac{1}{s}, \tag{1}$$

$$F(s) = \frac{v'(s)}{v(s)} = \frac{k}{s+k}, \tag{2}$$

$$S_I(t) = At, \quad t \geq 0, \tag{3}$$

$$S_F(t) = A - Ae^{-kt}, \quad t \geq 0, \tag{4}$$

where $I(s)$ and $F(s)$ are the transfer function of pure integrator and the closed-loop transfer function of FOS respectively. $A$ is the magnitude of the step input signal, and $S_{\mathrm{I}}(t)$ and $S_{\mathrm{F}}(t)$ are the step responses of (1) and (2) respectively.

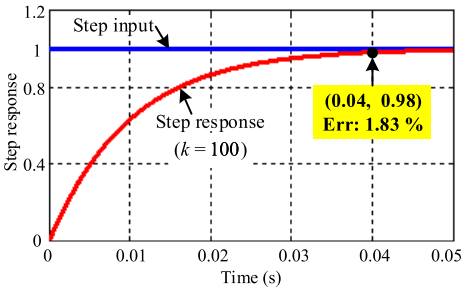


**FIGURE 4.** Step response of the FOS in Fig. 2.

It can be observed from (3) that the step response of the pure integrator behaves as an amplitude integration of the input. As for the step response of FOS in (4), it contains two terms: a steady-state term equal to the input and an attenuation term with a time constant $1/k$. The step response of FOS is further plotted in Fig. 4, where it is noted that the output converges to the input gradually, showing the dc-tracking characteristic of FOS. Moreover, it can be seen from Fig. 4 and calculated from (4) that the error between the input and the output of FOS is 1.83% at the time $4/k$ which is defined in [46] as the settling time $t_{\mathrm{s}}$ of FOS for dc-signal tracking.

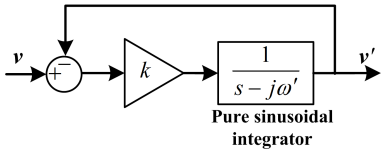


**FIGURE 5.** Block diagram of the sinusoidal FOS (SFOS) for sinusoidal-signal extraction.

### B. PURE SINUSOIDAL INTEGRATOR AND SINUSOIDAL FOS

The FOS in Fig. 2 is not suitable for tracking sinusoidal signal due to the finite gain of pure integrator at non-zero frequencies. To track a sinusoidal signal with frequency $\omega'$, the infinite gain of pure integrator should be shifted to $\omega'$, resulting in a Pure Sinusoidal Integrator (PSI) and a sinusoidal FOS (SFOS) in Fig. 5. The transfer function of the PSI is written as

$$SI\,(s) = \frac{1}{s - j\omega'}, \tag{5}$$

and its magnitude/phase-frequency characteristics are shown in Fig. 6. The closed-loop transfer function of the SFOS can then be given by

$$SF\,(s) = \frac{v'(s)}{v(s)} = \frac{k}{s - j\omega' + k}. \tag{6}$$

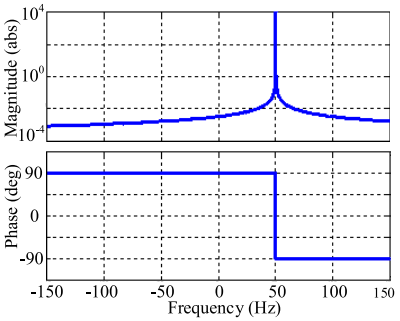


**FIGURE 6.** Magnitude/phase-frequency characteristics of the pure sinusoidal integrator (PSI).

To investigate the characteristics of PSI and SFOS, their "step responses" are derived. The "step input" signal is a complex vector given by

$$\begin{aligned} \boldsymbol{v}\,(t) &= v_{\alpha}\,(t) + jv_{\beta}\,(t) \\ &= A\cos\left(\omega' t + \varphi\right) + jA\sin\left(\omega' t + \varphi\right), \end{aligned} \tag{7}$$

where $A$, $\omega'$ and $\varphi$ are the amplitude, angular frequency, and initial phase of the "step input" signal. The responses of PSI and SFOS have been derived in the Appendix. The results are given here by

$$S_{SI}\,(t) = At\cos\left(\omega' t + \varphi\right) + jAt\sin\left(\omega' t + \varphi\right) t \geq 0 \tag{8}$$

$$\begin{aligned} S_{SF}\,(t) = {} & A\left(1 - e^{-kt}\right)\cos\left(\omega' t + \varphi\right) \\ & + jA\left(1 - e^{-kt}\right)\sin\left(\omega' t + \varphi\right) t \geq 0 \end{aligned} \tag{9}$$

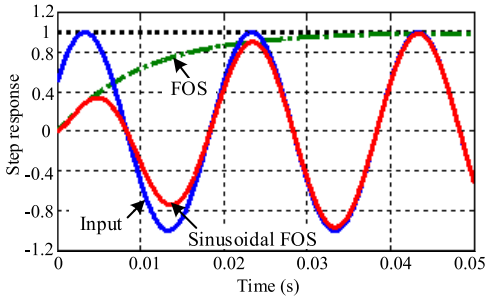


**FIGURE 7.** "Step response" of the SFOS.

From (8), it can be seen that the response of the PSI also behaves as the amplitude integration of the input, which is consistent with the pure integrator for dc signal. Further, the response of the SFOS in (9) is consistent with that of the FOS in (4), which contains a steady-state term and an attenuation term. The response is further shown in Fig. 7, where it is noted that the output signal converges to the input gradually due to the amplitude integration characteristic of the PSI. Besides, the amplitude response of the SFOS follows the FOS all the time, which means that they share the same settling time $t_{\mathrm{s}}$. Hence, the FOS can be looked as a special SFOS when its working frequency is shifted to 0.

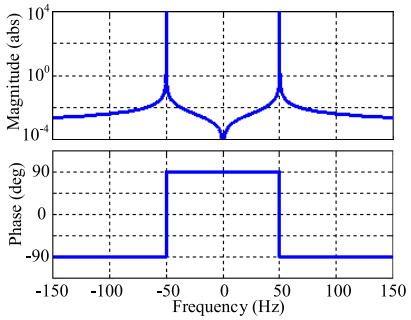


**FIGURE 8.** Magnitude/phase-frequency characteristics of the symmetrical sinusoidal integrator (SSI).

### C. SYMMETRICAL SINUSOIDAL INTEGRATOR AND SYMMETRICAL SINUSOIDAL FOS

The SFOS in Fig. 5 can realize sinusoidal signal estimation, yet it needs complex vector inputs. The complex vector can be easily obtained in a three-phase system, while it is not convenient for a single-phase system. One solution is to combine a positive- and a negative-sequence PSI into a Symmetrical Sinusoidal Integrator (SSI, also denoted as GI in [12]) expressed by (10), which has two infinite gains at both positive and negative frequencies as shown in Fig. 8.

$$SSI\ (s) = \frac{1}{s - j\omega'} + \frac{1}{s + j\omega'} = \frac{2s}{s^2 + \omega'^2} \tag{10}$$

For an input sinusoidal signal with a positive frequency $v(t) = A\sin(\omega' t + \varphi)$, the response of the SSI is expressed by (11), which contains not only an amplitude-integration term, but also an additional term generated by the negative-sequence PSI. Obviously, the second term in (11) will be much smaller than the first term as time going by, and thus the SSI still inherits the magnitude integration characteristic of the PSI.

$$S_{SSI}\ (t) = At\sin\left(\omega' t + \varphi\right) + \frac{A\sin\left(\omega' t\right)\sin\varphi}{\omega'} \tag{11}$$

$$SSF\ (s) = \frac{v'(s)}{v(s)} = \frac{2ks}{s^2 + 2ks + \omega'^2} \tag{12}$$

Block diagram of the Symmetrical Sinusoidal FOS (SSFOS) built by SSI is shown in Fig. 9, whose closed-loop transfer function is given by (12). The SSFOS can track sinusoidal signal (with either positive or negative frequency) due to the infinite gain of SSI at the desired frequency. To illustrate it, the ''step response'' of (12) is derived in (13), as shown at the bottom of this page, and shown in Fig. 10. Compared with (9), (13) has the same steady-state term but a different attenuation term. Specially, when $k$ is much smaller than $\omega'$, (13) can be simplified to (14), as shown at the bottom of this page, which is similar to (9), except for an exponential attenuation term. The SSFOS has actually a second-order transfer function. It is named as ''first order'' since it approximately shows an FOS characteristic in its magnitude response for sinusoidal signal tracking.

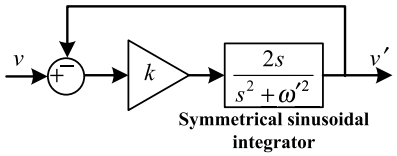


**FIGURE 9.** Block diagram of the symmetrical sinusoidal FOS (SSFOS) for sinusoidal-signal extraction.

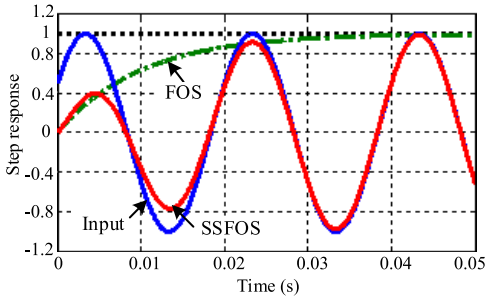


**FIGURE 10.** ''Step response'' of the SSFOS.

## III. RE-INVESTIGATION OF GI-BASED FILTERS FROM FOS PERSPECTIVE

In this Section, with the help of the above three FOSs, a re-investigation of several classical GI-based filters is carried out, which provides not only the convenience for parameter design of these methods, but also a generalized way to investigate their working principles.

### A. GI-BASED QSG

The structure of GI-QSG (also named as SOGI-QSG in [47]) is shown in Fig. 11 with its transfer functions expressed in (15) and (16), where the former shows that $v'$ is the band-pass-filter version of the input with a unity gain and zero phase-shift at the frequency of $\omega'$. In contrast, $qv'$ is the low-pass-filter version of the input with a unity gain and 90° phase-shift at the frequency of $\omega'$ [48]. Quadrature signals can thus be obtained by this structure, which can be used for

$$S_{SSF}\ (t) = A\sin\left(\omega' t + \varphi\right) + A\frac{\sin\left(t\sqrt{\omega'^2 - k^2}\right)\left(-\omega'\cos\varphi + k\sin\varphi\right)}{\sqrt{\omega'^2 - k^2}}e^{-tk} - A\sin\varphi\cos\left(t\sqrt{\omega'^2 - k^2}\right)e^{-tk} \quad t \geq 0 \tag{13}$$

$$S_{SSF}\ (t) \approx A\left(1 - e^{-tk}\right)\sin\left(\omega' t + \varphi\right) + \frac{A\sin\left(\omega' t\right)k\sin\varphi}{\omega'}e^{-tk} \quad t \geq 0 \tag{14}$$

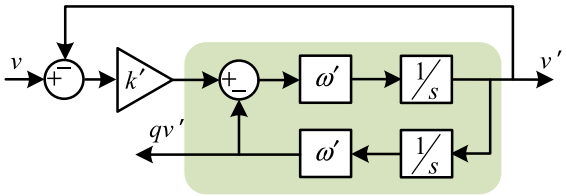


**FIGURE 11.** Block diagram of the generalized integrator based quadrature signal generator (GI-QSG).

frequency estimation [17] and grid synchronization [47].

$$D(s) = \frac{v'(s)}{v(s)} = \frac{k'\omega' s}{s^2 + k'\omega' s + \omega'^2}, \tag{15}$$

$$Q(s) = \frac{qv'(s)}{v(s)} = \frac{k'\omega'^2}{s^2 + k'\omega' s + \omega'^2}. \tag{16}$$

The principle of the GI-QSG is actually the same with the SSFOS. To illustrate it, the SSI in (10) is rewritten as

$$SSI(s) = \frac{2s}{s^2 + \omega'^2} = \frac{2}{\omega'} \frac{\omega'/s}{1 + \omega'^2/s^2}. \tag{17}$$

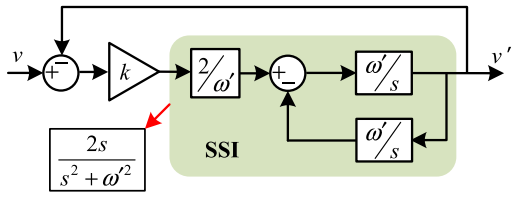


**FIGURE 12.** Equivalent block diagram of the SSFOS.

The right-side term in (17) can be looked as the closed-loop transfer function of a system with the gain $\omega'/s$ in both its forward path and feedback path. In this case, the SSI can be represented using block diagrams, which when used to replace the SSI in Fig. 9, resulting in a new structure of SSFOS in Fig. 12. It is noted that the structure is actually the same with the GI-QSG as long as $k$ is set to $k'\omega'/2$. Hence, the GI-QSG is equivalent to the SSFOS, and the parameter design of GI-QSG can refer to that of SSFOS as well.

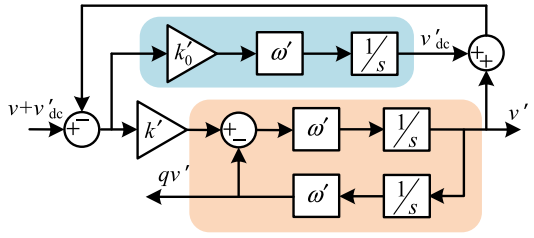


**FIGURE 13.** Block diagram of the modified GI-QSG for dc rejection.

### B. MODIFIED GI-QSG

Because $qv'$ is the low-pass-filter version of the input, GI-QSG is sensitive to any input dc component [41], [44],

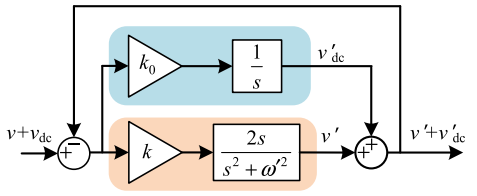


**FIGURE 14.** Block diagram of the SSFOS combined with a FOS.

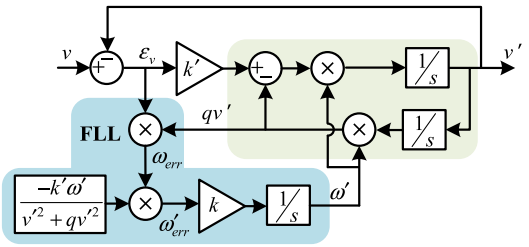


**FIGURE 15.** Block diagram of the GI-based frequency-locked loop (FLL).

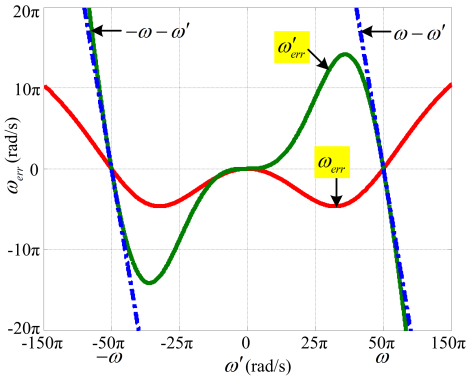


**FIGURE 16.** Behavior of $\omega_{err}$ and $\omega'_{err}$ with the changing of $\omega'$ in Fig. 17 when the integrator of FLL is disabled.

which can be introduced by the amplifier or the A/D conversion process. To overcome the drawback, a modified GI-QSG was proposed in [41], whose structure is shown in Fig. 13 with an integrator added to the GI-QSG. As a result, the input dc component can be extracted to $v'_{dc}$ in steady state and both $v'$ and $qv'$ will not contain dc offset anymore.

The principle of the modified GI-QSG can be explained by the FOS concept. In Fig. 14, an FOS and an SSFOS are combined with a common feedback. By referring to the equivalence between SSFOS and GI-QSG, it is easy to find that the combined system in Fig. 14 is equivalent to the structure of the modified GI-QSG with $k = k'\omega'/2$ and $k_0 = k'_0\omega'$. Parameter design of the modified GI-QSG can therefore refer to that of FOS and SSFOS.

### C. GI-BASED FLL

To make the GI-QSG frequency-adaptive, either PLL [15] or FLL [17] can be used to estimate the frequency of the input. Compared with the GI-PLL in [15], neither phase angle nor trigonometric functions are used in GI-FLL. The structure of GI-FLL is shown in Fig. 15, and the averaged characteristic of the variable $\omega_{err}$ can be described by

$$\omega_{err} \approx \frac{A^2 |D(j\omega)|^2}{2k'\omega^2} \left(\omega'^2 - \omega^2\right), \tag{18}$$

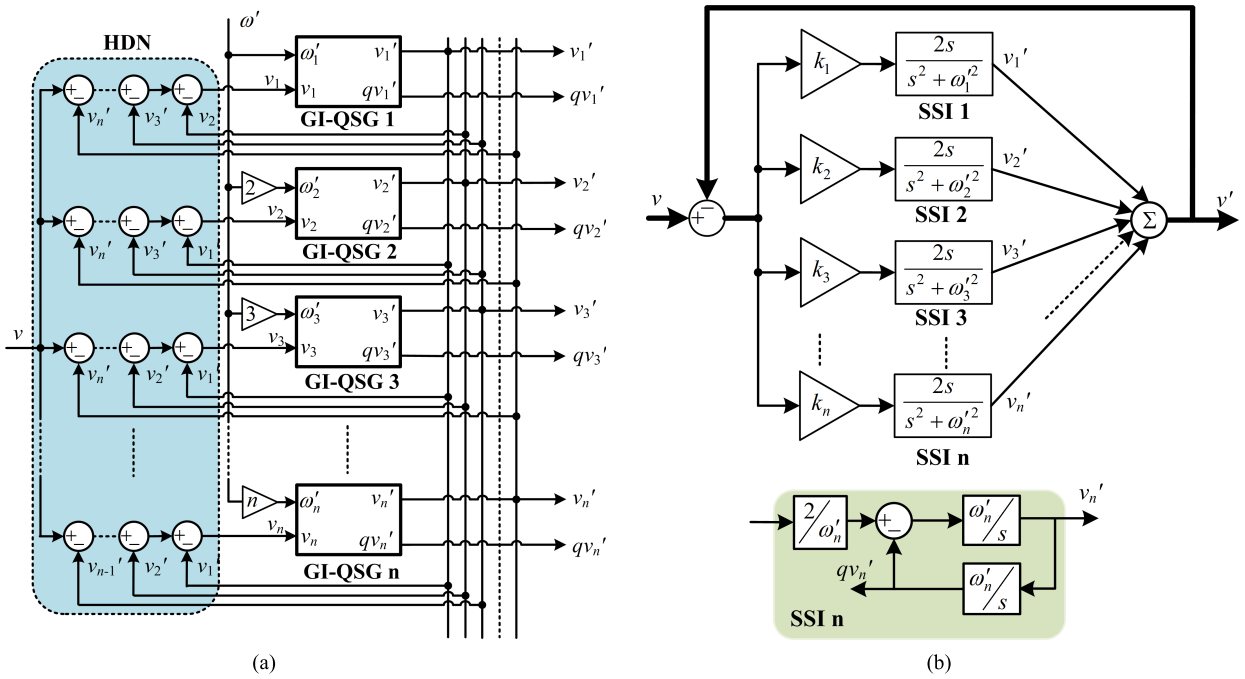


**FIGURE 17.** Block diagrams of multiple GI-QSG (MGI-QSG), (a) conventional MGI-QSG block diagram, and (b) equivalent MGI-QSG block diagram based on FOS concept.

where $A$, and $\omega$ are the magnitude and frequency of the input sinusoidal signal, and $|D(j\omega)|$ is the magnitude-frequency characteristic of (15) [23]. To investigate the behavior of $\omega_{err}$, an example is taken by setting $A$, $k'$ and $\omega$ to 10, $\sqrt{2}$, and $100\pi$ rad/s respectively. Firstly, the integrator of FLL is disabled, and the frequency $\omega'$ is artificially changed from $-150\,\pi$ rad/s to $150\,\pi$ rad/s. The value of $\omega_{err}$ is then plotted in Fig. 16 with the changing of $\omega'$. It is noted that, above 0, $\omega_{err}$ is negative when $0 < \omega' < \omega$ and positive when $\omega' > \omega$. This mechanism is opposite to that of the frequency error signal of an FOS (see the dash-dot line in Fig. 16). An integrator with a negative gain should be placed between $\omega_{err}$ and $\omega'$ in Fig. 15 in order to force $\omega_{err}$ to zero in steady state.

Despite the similarity of FLL and FOS, the dynamic characteristic of FLL in (18) is nonlinear, which makes the parameter design of FLL quite difficult in practice. A normalization method was thus proposed in [23] to solve the problem, whose principle can be explained by

$$\omega'_{err} = \omega_{err}\frac{-k'\omega'}{A^2} \approx \omega - \omega', \tag{19}$$

where $A^2$ can be calculated by $v'^2 + qv'^2$ in steady state. It is interesting to find that the mechanism of (19) is the same with that in FOS. It means that, after normalization, the FLL is equivalent to an FOS, which can also be found by comparing the curve of $\omega'_{err}$ (for FLL) and $\omega - \omega'$ (for FOS) in Fig. 16.

### D. MULTIPLE GI-QSG

Although the GI-QSG has strong attenuation to high-order harmonics, it is quite sensitive to low-order harmonics which are close to the fundamental frequency [25]. To overcome the drawback, the Multiple GI-QSG (MGI-QSG, denoted as MSOGI-QSG in [25]) was proposed in [25], which contains a Harmonic-Decoupling Network (HDN) and parallel GI-QSGs for harmonic extraction as shown in Fig. 17(a). Herein, the SSFOS is used to illustrate the principle of MGI-QSG.

To begin with, taking the first channel in HDN as an example, it is noted that the harmonic components estimated by other channels are subtracted from the input of the first channel. Inside each GI-QSG block, $v'$ has been subtracted from its reference $v$. In this case, if the feedback point of $v'$ inside each GI-QSG is moved into HDN, all channels in HDN will become the same, i.e. subtract the summation of all the components from $v'_1$ to $v'_n$. Next, by moving the summation operator behind the GI-QSG blocks, the structure in Fig. 17(b) can be obtained by further considering the equivalence between GI-QSG and SSFOS, which is actually a combination of several SSFOSs with a common feedback. The principle of MGI-QSG can thus be understood easily.

### E. SEQUENCE FILTER

The structure of SF is shown in Fig. 18(a), which was first presented in [11] for extracting either positive- or negative-sequence component. The SF is actually the same with the Complex-Coefficient Filter (CCF) proposed in [38], whose structure is shown in Fig. 18(b). Both the SF and the CCF are essentially the same with the SFOS. To illustrate it, the PSI in (5) is rewritten in a more convenient form of

$$SI(s) = \frac{1}{s - j\omega'} = \frac{1/s}{1 - j\omega'/s}. \tag{20}$$

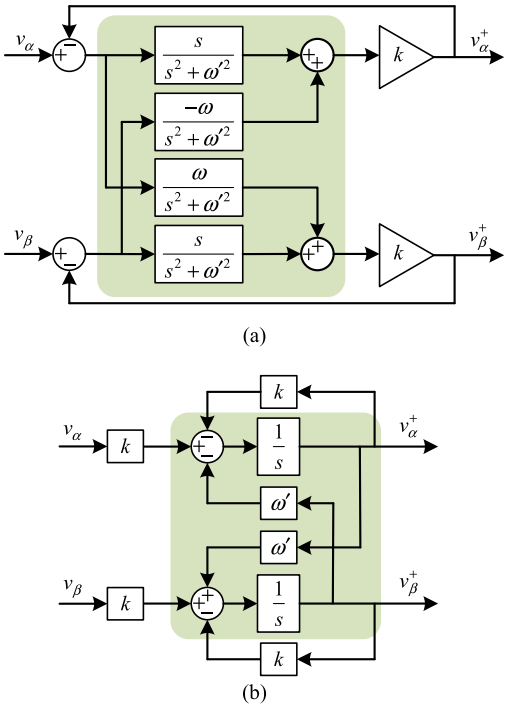


**FIGURE 18.** Block diagrams of (a) the Sequence Filter (SF) in [12] and (b) the complex-coefficient filter in [38].

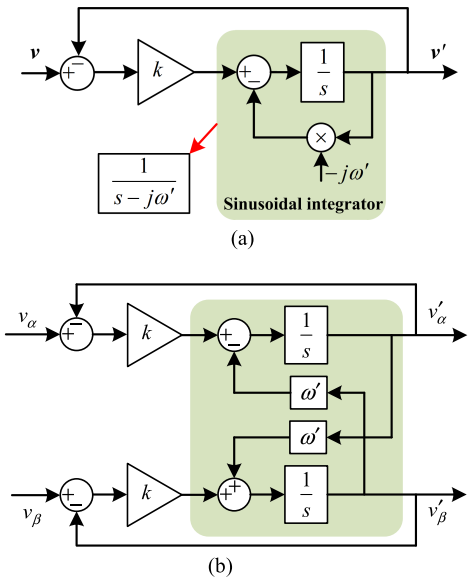


**FIGURE 19.** Block diagrams of the SFOS (a) implemented with pure integrator, and (b) when $j$ is implemented by a cross-coupling term.

The right-side term of (20) can be looked as the closed-loop transfer function of a system with the gain $1/s$ in its forward path and the gain $-j\omega'$ in its feedback path. When the diagram of the closed-loop system is used to replace the PSI in Fig. 5, a new structure of SFOS can be obtained as shown in Fig. 19(a). Further, in a three-phase system, the constant $j$ in Fig. 19(a) can be implemented by a cross-coupling term in Fig. 19(b). It is noted that the structure in Fig. 19(b) is equivalent to the CCF in Fig. 18(b), i.e. the CCF is essentially an SFOS. Moreover, the PSI in (5) can also be written as

$$SI\,(s) = \frac{1}{s - j\omega'} = \frac{s + j\omega'}{s^2 + \omega'^2} = \frac{s}{s^2 + \omega'^2} + j\frac{\omega'}{s^2 + \omega'^2}. \tag{21}$$

It is noted that the shaded part in Fig. 18(a) is actually the block representation of the right term of (21) [43]. The SF is therefore equivalent to the SFOS as well. In this case, the "step response" in Fig. 7 and (9) can be used to describe the characteristics of SF and CCF, for which, the amplitude error between the step input and the output is 1.83% at the time $4/k$ which can be looked as the settling time of SF and CCF.

It should be pointed out that the SF can also be configured for dc-offset rejection [42], frequency estimation [39], and harmonic extraction [36], [37], whose structures are similar to the modified GI-QSG, GI-FLL, and MGI-QSG, respectively. Similarly, these structures can be explained by the FOS concept as well, which will be not elaborated in this paper.

## IV. SECOND-ORDER SF AND SECOND-ORDER GI-QSG

The FOS concept is helpful not only for understanding the principle of GI-based filters, but also for deriving improved structures. For example, it is well known that high-order system usually has better filtering characteristic than first-order system. The "Second-Order" GI-based filters can therefore be proposed for enhancing the harmonic attenuation performance.

### A. STANDARD SECOND-ORDER SYSTEM

The transfer function of the standard Second-Order System (SOS) is given by (22), where $\zeta$ and $\omega_n$ represent the damping ratio and the undamped natural frequency of SOS [46]. Step response of the standard SOS can then be expressed as (23), where the settling time $t_s = 4.4/(\zeta\omega_n)$ is the instant at which the error between the input and the output falls below 2% [46].

$$S\,(s) = \frac{\omega_n^2}{s^2 + 2\zeta\omega_n s + \omega_n^2} \tag{22}$$

$$S_s\,(t) = A\left(1 - \frac{\sin\,(\omega_d t + \beta)}{\sqrt{1-\zeta^2}} e^{-\zeta\omega_n t}\right), \quad t \geq 0 \tag{23}$$

where $\omega_d = \omega_n\sqrt{1-\zeta^2}$, and $\beta = \arccos\zeta$ [46].

The block diagram of the standard SOS is shown in Fig. 20(a), where its open-loop transfer function is found to contain a first-order inertia element. This element has the same transfer function with the FOS in (2), and can hence be replaced by it to obtain Fig. 20(b) needed for later sections.

### B. SECOND-ORDER SF

The difference between the FOS in Fig. 2 and the SFOS in Fig. 5 is their integrators, which are the PSI in Fig. 5 instead of pure integrators in Fig. 2. Similarly, the pure integrators in Fig. 20(b) can also be replaced by two sinusoidal integrators, which then leads to the proposed SO-SF structure shown

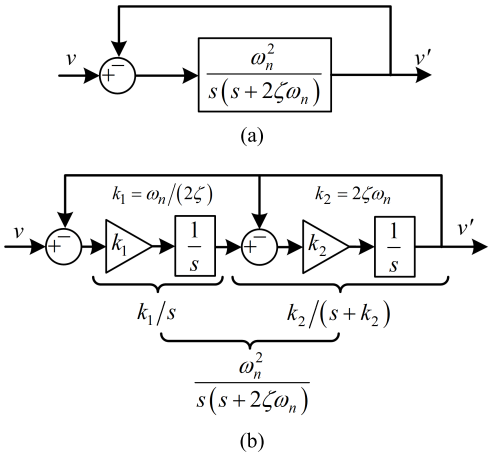


**FIGURE 20.** Block diagrams of the SOS, (a) block diagram implemented with open-loop transfer function, and (b) block diagram implemented with two pure integrators.

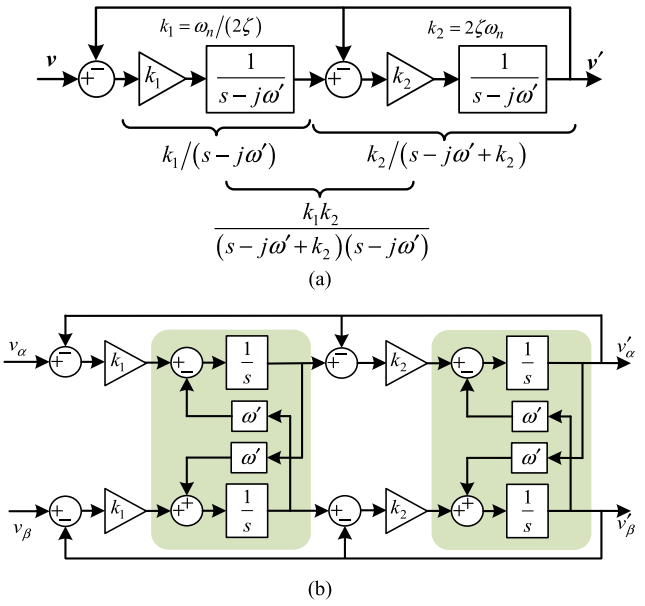


**FIGURE 21.** Block diagrams of the Second-Order SF (SO-SF), (a) implemented with two PSIs, and (b) when $j$ in PSI implemented by a cross-coupling term.

in Fig. 21(a), where $\zeta$ is the damping ratio of the SO-SF in terms of magnitude response of the sinusoidal signal. For an easy implementation, Fig. 21(a) is redrawn as Fig. 21(b) based on the equivalence established by Fig. 5 and Fig. 19(b).

To prove the consistence of the response between SOS and SO-SF, an input signal $\boldsymbol{v}(t) = \cos(100\pi t + \pi/6) + j\sin(100\pi t + \pi/6)$ is applied to the SO-SF. Its response with $\zeta = 0.707$ and $\omega_n = 77.8$ rad/s is shown in Fig. 22. For comparison, responses of the corresponding SOS and FOS are plotted in Fig. 22 as well. It is noted that the magnitude response of the SO-SF always follows the response of the SOS when their parameters are the same, verifying the correctness of the analysis.

To evaluate the performance of the proposed SO-SF, its magnitude-frequency response is derived. First, according

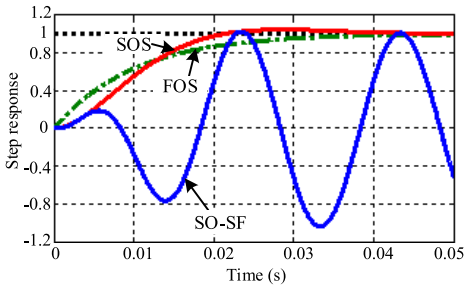


**FIGURE 22.** Step response of SO-SF compared with that of FOS and SOS.

to Fig. 21(a), the open-loop complex transfer function of the SO-SF can be expressed as

$$O_1(s) = \frac{k_1 k_2}{(s - j\omega' + k_2)(s - j\omega')} \tag{24}$$

The closed-loop complex transfer function can therefore be derived as

$$C_1(s) = \frac{O_1(s)}{1 + O_1(s)} = \frac{k_1 k_2}{(s - j\omega' + k_2)(s - j\omega') + k_1 k_2} \tag{25}$$

The magnitude of (25) is given by

$$|C_1(j\omega)| = \frac{k_1 k_2}{\sqrt{\left(k_1 k_2 - (\omega - \omega')^2\right)^2 + k_2^2 (\omega - \omega')^2}} \tag{26}$$

Besides, for the SF, the magnitude of its closed-loop transfer function can be derived from (6) as

$$|F_\omega(j\omega)| = \frac{k}{\sqrt{k^2 + (\omega - \omega')^2}} \tag{27}$$

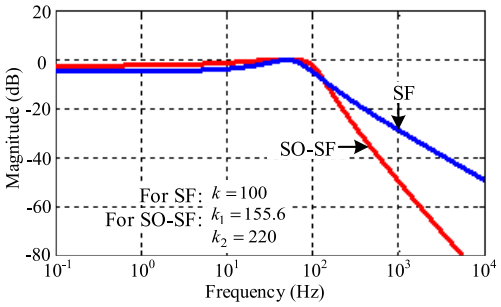


**FIGURE 23.** Magnitude-frequency plots of the SF and the SO-SF.

Taking $\omega' = 100\,\pi$ rad/s as an example, the magnitude responses of (26) and (27) are drawn in Fig. 23, where $k$ is set to 100 for SF, yet for SO-SF, $k_1$ and $k_2$ are set to 155.6 and 220 respectively to ensure the same settling time with SF. It can be observed from Fig. 23 that the proposed SO-SF has stronger attenuation than the SF above the fundamental frequency. On the other hand, below the fundamental frequency, the attenuation performance of SO-SF is slightly weaker than SF, which makes it a bit more sensitive to subharmonics and dc offset. In this case, the SO-SF is not very predominant

in practice, which can just be regarded as an alternative way of implementing the SF.

### C. SECOND-ORDER GI-FLL

Similar to SO-SF, a Second-Order GI-QSG (SO-GI-QSG) structure can be proposed. It is now configured with an FLL to make it frequency-adaptive and the overall algorithm is thus named as SO-GI-FLL, whose structure is shown in Fig. 24.

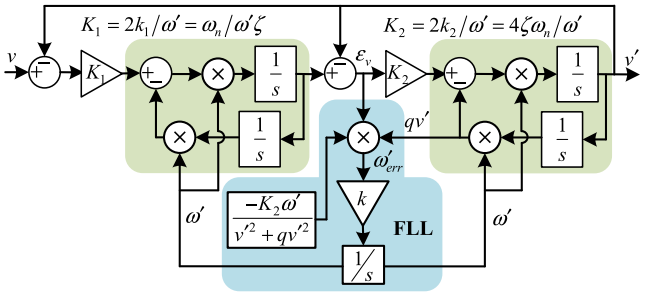


**FIGURE 24.** Block diagram of Second-Order GI-FLL implemented with two pure integrators.

The open-loop transfer function of the SO-GI-QSG can be given as

$$O_2(s) = \frac{K_1 K_2 \omega'^2 s^2}{\left(s^2 + K_2\omega' s + \omega'^2\right)\left(s^2 + \omega'^2\right)} \tag{28}$$

Then, the transfer functions for relating the input $v$ to the in-quadrature outputs can be derived as

$$\begin{aligned} D_2(s) &= \frac{v'(s)}{v(s)} = \frac{O_2(s)}{1 + O_2(s)} \\ &= \frac{K_1 K_2 \omega'^2 s^2}{\left(s^2 + K_2\omega' s + \omega'^2\right)\left(s^2 + \omega'^2\right) + K_1 K_2 \omega'^2 s^2} \end{aligned} \tag{29}$$

$$\begin{aligned} Q_2(s) &= \frac{qv'(s)}{v(s)} = D_2 \frac{\omega'}{s} \\ &= \frac{K_1 K_2 \omega'^3 s}{\left(s^2 + K_2\omega' s + \omega'^2\right)\left(s^2 + \omega'^2\right) + K_1 K_2 \omega'^2 s^2} \end{aligned} \tag{30}$$

It can be seen from (29) and (30) that the SO-GI-QSG has actually a fourth-order transfer function. It is named as "second order" since it is derived from SOS and showing a second-order characteristic in terms of magnitude. The SO-GI-QSG has a better filtering characteristic than GI-QSG because of its higher order. To illustrate this, Bode diagrams of (29) and (30) are drawn in Figs. 25(a) and (b) respectively which are compared with the Bode diagrams obtained by (15) and (16). The gain $k'$ of GI-QSG is set to $\sqrt{2}$. With the same settling time, $K_1$ and $K_2$ of the SO-GI-QSG can be calculated to be 1.56 and 3.11 respectively. It can be observed from Figs. 25(a) and (b) that the SO-GI-QSG has stronger attenuation ability for both low- and high-frequency components than GI-QSG, which validates the correctness of the original guess. As for the FLL, its structure and working

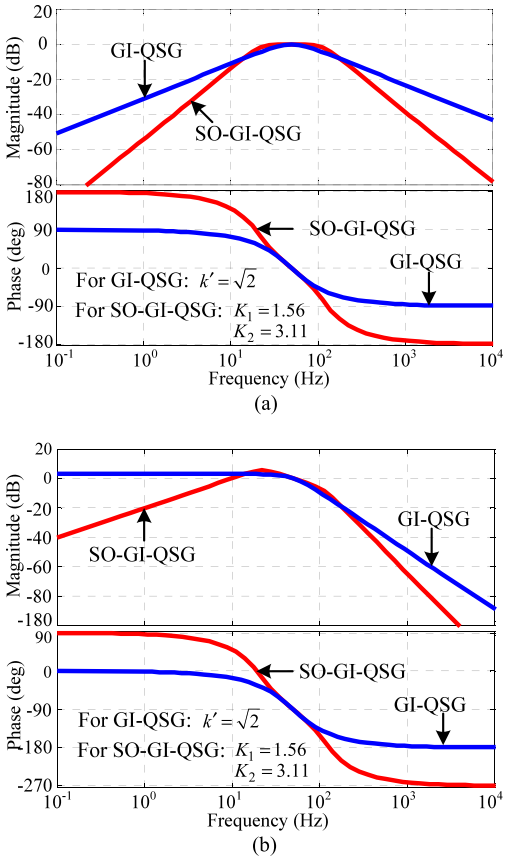


**FIGURE 25.** Bode diagrams of the GI-QSG and SO-GI-QSG for relating (a) in-phase output $v'$ to input $v$, and (b) quadrature output $qv'$ to input $v$.

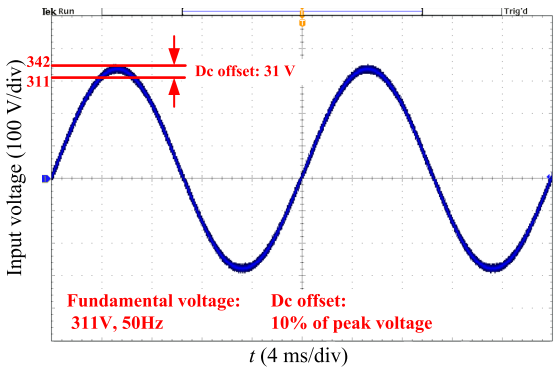


**FIGURE 26.** Sampled grid voltage with dc offset.

principle are the same with those of the FLL in Fig. 15, except that the gain in the normalization block should be changed from $k'$ to $K_2$ accordingly. Theoretical analysis can refer to the content in Section III (C), which is not elaborated again in this section. Evaluation of the performance of FLL under harmonic and dc components will be provided in next section.

## V. EXPERIMENTAL VERIFICATION

An experimental setup consisting of a grid simulator Chroma 61845, a dSPACE DS1007 platform, a DS2004 high-speed

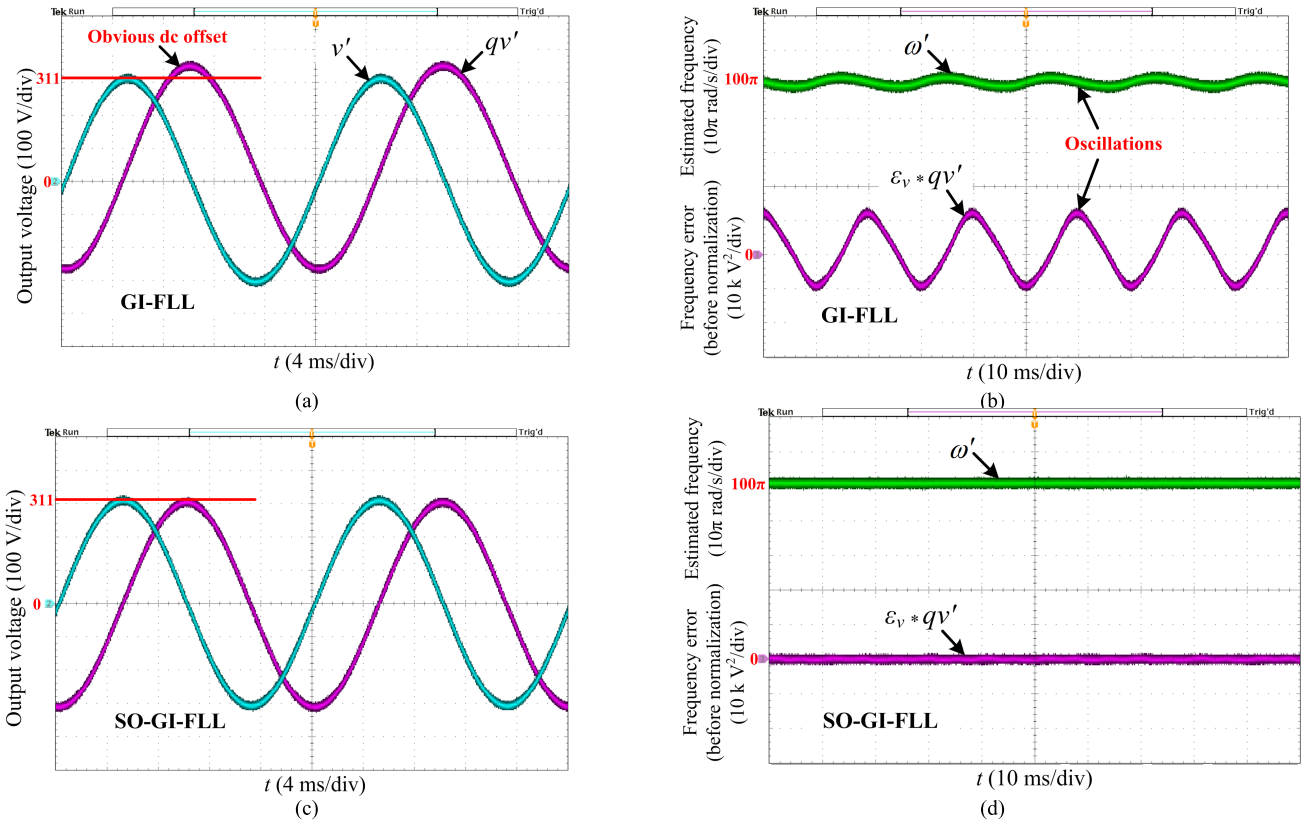


**FIGURE 27.** Experimental output waveforms when the input voltage contains dc offset, (a) the in-quadrature output waveforms obtained with GI-QSG, (b) the estimated frequency and frequency error waveforms obtained with GI-QSG, (c) the in-quadrature output waveforms obtained with SO-GI-QSG, (d) the estimated frequency and frequency error waveforms obtained with SO-GI-QSG.

A/D board, a DS2102 high-resolution D/A board and a voltage sampling board has been used. The grid simulator is used to generate the required voltage which is then sensed by the voltage senor board and sampled by the DS2004 A/D board. The sampled signal is next processed by the proposed SO-GI-QSG and the conventional GI-QSG which are implemented in dSPACE with the sampling frequency of 10 kHz. The two integrators of SSI are discretized by forward Euler and backward Euler respectively according to [49]. The estimated variables are converted to analog signal through the DS2102 D/A board and the waveforms are displayed in oscilloscope eventually.

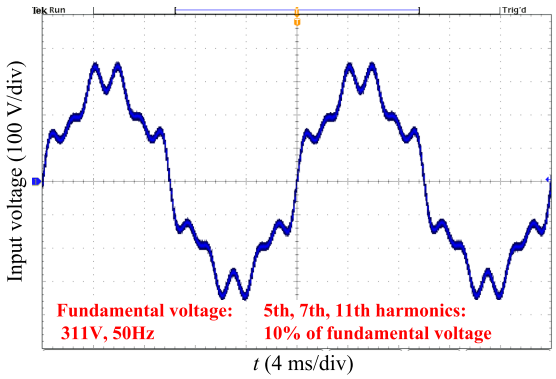


**FIGURE 28.** Sampled grid voltage with harmonics.

### A. STEADY-STATE PERFORMANCE

Two experiments are performed in this part to evaluate the performances of the proposed SO-GI-FLL when the sampled grid voltage contains dc component and harmonic components. Corresponding results of GI-FLL (or SOGI-FLL) are also provided for comparison.

Waveform of the sampled grid voltage with dc offset is shown in Fig. 26, where the frequency of the fundamental grid voltage is 50 Hz and its root-mean-square value is 220 V with a dc offset equal to 10% of the peak grid voltage. Fig. 27(a) shows waveforms of the in-quadrature signals generated by GI-FLL, from where it is noted that the output $qv'$ of GI-FLL contains an obvious offset due to the low-pass characteristic of $Q(s)$ derived in (16). Further, for frequency estimation, the dc component in $qv'$, after been multiplied by $\varepsilon_v$, will produce an ac component as well in the frequency error signal $\omega_{err}$. This ac component can further cause error in the estimated frequency after integration. Experimental waveforms of the frequency error ($\omega_{err} = \varepsilon_v qv'$) and the estimated frequency are shown in Fig. 27(b), both of which contain obvious ac components, and therefore validate the correctness of the theoretical analysis. In comparison, waveforms of the in-quadrature outputs for SO-GI-FLL are shown in Fig. 27(c),

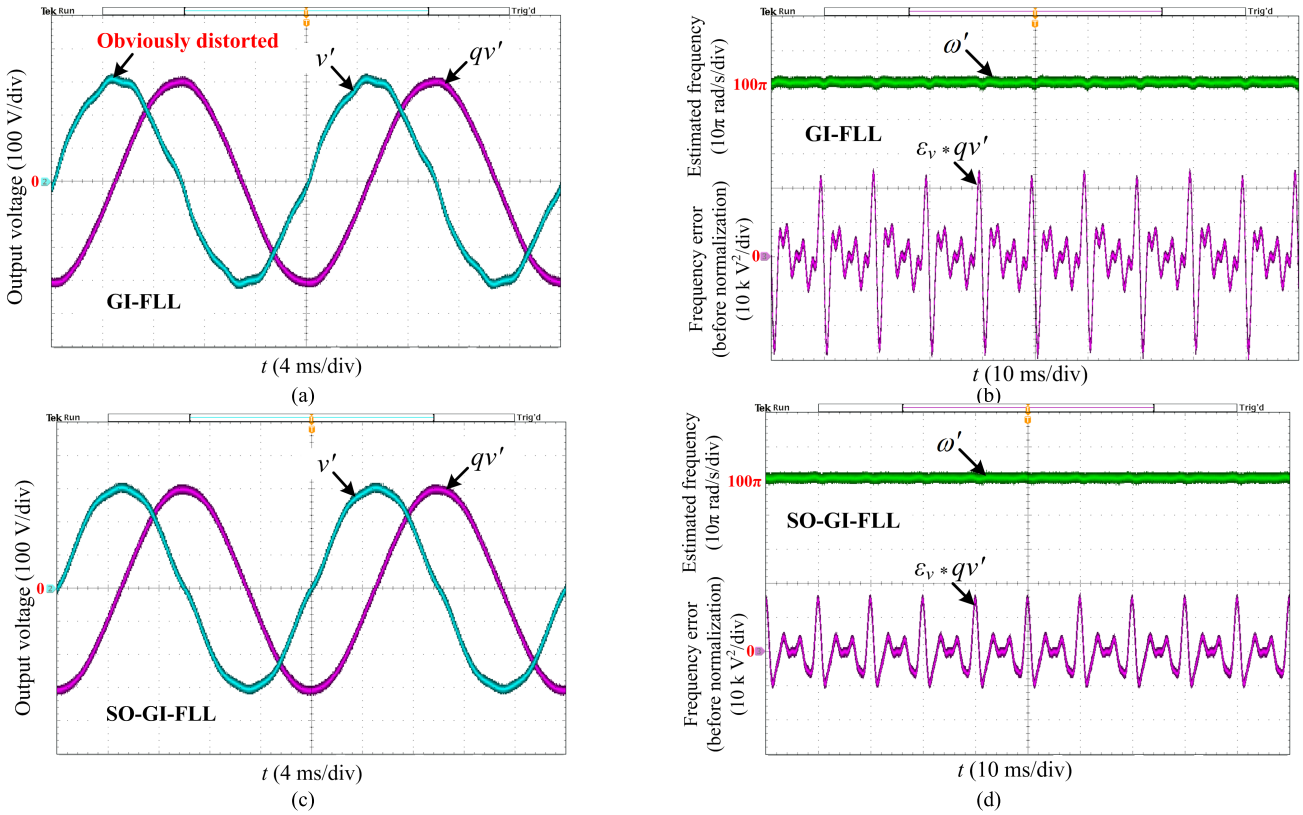


**FIGURE 29.** Experimental output waveforms when the input voltage contains harmonics, (a) the in-quadrature output waveforms obtained with GI-QSG, (b) the estimated frequency and frequency error waveforms obtained with GI-QSG, (c) the in-quadrature output waveforms obtained with SO-GI-QSG, (d) the estimated frequency and frequency error waveforms obtained with SO-GI-QSG.

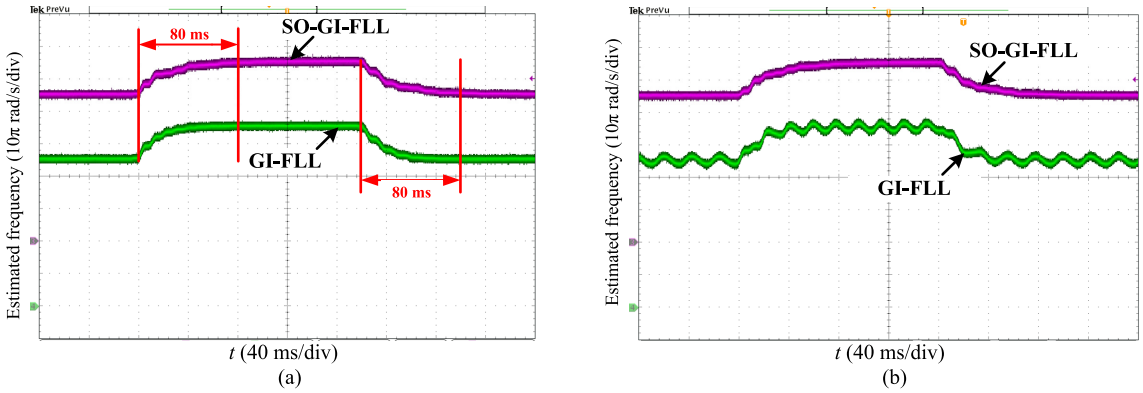


**FIGURE 30.** Dynamic responses of the two FLLs in the presence of a frequency step (from 45 Hz to 55 Hz), (a) input signal without dc offset, and (b) input signal with dc offset.

where the dc component has been effectively attenuated in both $v'$ and $qv'$. As a result, in steady state, the frequency error of SO-GI-FLL is approximately 0 and the estimated frequency is accurately $100\pi$ rad/s as observed from Fig. 27(d), showing an excellent performance of the proposed SO-GI-FLL to GI-FLL in suppressing the dc offset.

In the second experiment, performances of SO-GI-FLL and GI-FLL under distorted grid voltage are compared. Fig. 28 shows the waveform of the distorted grid voltage, where the fundamental component keeps the same with that in the first experiment, while the dc offset is replaced by the typical $5^{th}$, $7^{th}$ and $11^{th}$ order harmonics whose magnitudes are all 10% of the fundamental component. Figs. 29(a) and (c) show the in-quadrature output waveforms of GI-FLL and SO-GI-FLL respectively. Clearly, the GI-FLL does not produce satisfactory harmonic attenuation at its $v'$ output. In comparison, the waveforms produced by SO-GI-FLL are less distorted than GI-FLL, due to its stronger

attenuation ability which has been shown with Bode diagrams in Fig. 25. Furthermore, the frequency error signal produced by SO-GI-FLL is also less distorted than GI-FLL, which leads to a smoother estimated frequency by comparing Figs. 29(b) and (d).

Therefore, the measured results in these two experiments match well with the theoretical analysis performed using Bode diagrams in Fig. 25, i.e. the proposed SO-GI-FLL shows superior performance to the conventional GI-FLL.

### B. DYNAMIC PERFORMANCE

To investigate the dynamic performance of FLL, a sudden jump in the grid frequency from 45 Hz to 55 Hz was generated by programming the ac-power source. The detected frequency by the GI-FLL and SO-GI-FLL are shown in Fig. 30(a), where the FLL gains $k$ for these two methods are both set to 50, resulting in a settling time of $t_s = 80$ ms according to the analysis in Section II(A). The results in Fig. 30(a) show that the frequency estimation of SO-GI-FLL has an FOS characteristic as well like the GI-FLL, and thus they have a similar dynamic performance. Experimental results when the grid voltage contains a dc offset are shown in Fig. 30(b). It is noted that the frequency estimated by GI-FLL suffers from oscillations, while the proposed SO-GI-FLL still keeps the performance like its steady-state, which means it eliminates the influence of the dc component. The dynamic performance comparisons of the two methods under harmonics are not further provided due to the limitation of the ac-power source.

## VI. CONCLUSION

The FOS concept is employed in this paper to perform a systematic re-evaluation of the GI-based filters, which not only gives intuitive illustrations about their principles, but also provides the possibility for developing new structures. Based on the FOS concept, an alternative SF and an improved QSG structure are proposed to enhance the filtering performance. An FLL is further added to the SO-GI-QSG to make it frequency adaptive. Due to the enhanced performance of SO-GI-QSG, the estimated frequency of SO-GI-FLL become less sensitive to the input harmonics and dc components than the conventional GI-FLL, which has been validated by experimental results.

Apart from the filters, the FOS concept can also be used to re-investigate the control systems using PR or PI controllers. High-order controllers can thus be tried for the control system as well, but additional considerations should be taken between the selectiveness and the stability of the control system.

## APPENDIX

With the Euler's formula and the angle-sum identity, (7) can be rewritten as

$$\begin{aligned} \boldsymbol{v}(t) &= A\cos\left(\omega' t+\varphi\right)+jA\sin\left(\omega' t+\varphi\right) \\ &= A\left(\cos(\varphi)+j\sin(\varphi)\right)\left(\cos\left(\omega' t\right)+j\sin\left(\omega' t\right)\right) \\ &= A\left(\cos(\varphi)+j\sin(\varphi)\right)e^{j\omega' t} \end{aligned} \tag{A.1}$$

The Laplace transform of (7) can be given by

$$\boldsymbol{v}(s) = A\left(\cos(\varphi)+j\sin(\varphi)\right)\frac{1}{s-j\omega'} \tag{A.2}$$

First, after passing through the pure sinusoidal integrator, the Laplace transform of the corresponding output can be given by

$$S_{SI}(s) = \boldsymbol{v}(s)\,SI(s) = A\left(\cos(\varphi)+j\sin(\varphi)\right)\left(\frac{1}{s-j\omega'}\right)^2 \tag{A.3}$$

The inverse-Laplace transform of (A.3) can be given by

$$\begin{aligned} S_{SI}(t) &= A\left(\cos(\varphi)+j\sin(\varphi)\right)te^{j\omega' t} \\ &= At\left(\cos(\varphi)+j\sin(\varphi)\right)\left(\cos\left(\omega' t\right)+j\sin\left(\omega' t\right)\right) \\ &= At\cos\left(\omega' t+\varphi\right)+jAt\sin\left(\omega' t+\varphi\right) \end{aligned} \tag{A.4}$$

Second, after passing through the sinusoidal FOS, the Laplace transform of the corresponding output can be given by

$$\begin{aligned} S_{SF}(s) &= \boldsymbol{v}(s)\,SF(s) \\ &= A\left(\cos(\varphi)+j\sin(\varphi)\right)\frac{1}{s-j\omega'}\frac{k}{s-j\omega'+k} \\ &= A\left(\cos(\varphi)+j\sin(\varphi)\right)\left(\frac{1}{s-j\omega'}-\frac{1}{s-j\omega'+k}\right) \end{aligned} \tag{A.5}$$

The inverse-Laplace transform of (A.5) can be given by

$$\begin{aligned} S_{SF}(t) &= A\left(\cos(\varphi)+j\sin(\varphi)\right)\left(e^{j\omega' t}-e^{j\omega' t-kt}\right) \\ &= A\left(\cos(\varphi)+j\sin(\varphi)\right)e^{j\omega' t}\left(1-e^{-kt}\right) \\ &= A\left(\cos(\varphi)+j\sin(\varphi)\right) \\ &\quad\times\left(\cos\left(\omega' t\right)+j\sin\left(\omega' t\right)\right)\left(1-e^{-kt}\right) \\ &= A\left(1-e^{-kt}\right)\cos\left(\omega' t+\varphi\right) \\ &\quad+jA\left(1-e^{-kt}\right)\sin\left(\omega' t+\varphi\right) \end{aligned} \tag{A.6}$$

## REFERENCES

[1] Y. Sato, T. Ishizuka, K. Nezu, and T. Kataoka, "A new control strategy for voltage type PWM rectifiers to realise zero steady-state control error in input current," in *Proc. Conf. Rec. IEEE-IAS Annu. Meeting*, Oct. 1997, pp. 1496–1503.

[2] Y. Sato, T. Ishizuka, K. Nezu, and T. Kataoka, "A new control strategy for voltage-type PWM rectifiers to realize zero steady-state control error in input current," *IEEE Trans. Ind. Appl.*, vol. 34, no. 3, pp. 480–486, May/Jun. 1998.

[3] D. N. Zmood and D. G. Holmes, "Stationary frame current regulation of PWM inverters with zero steady state error," in *Proc. IEEE 30th Annu. Power Electron. Spec. Conf.*, vol. 2. Jul. 1999, pp. 1185–1190.

[4] D. N. Zmood and D. G. Holmes, "Stationary frame current regulation of PWM inverters with zero steady-state error," *IEEE Trans. Power Electron.*, vol. 18, no. 3, pp. 814–822, May 2003.

[5] D. N. Zmood, D. G. Holmes, and G. Bode, "Frequency domain analysis of three phase linear current regulators," in *Proc. Conf. Rec. IEEE-IAS Annu. Meeting*, Oct. 1999, pp. 818–825.

[6] D. N. Zmood, D. G. Holmes, and G. H. Bode, "Frequency-domain analysis of three-phase linear current regulators," *IEEE Trans. Ind. Appl.*, vol. 37, no. 2, pp. 601–610, Mar./Apr. 2001.

[7] P. Mattavelli and S. Fasolo, "A closed-loop selective harmonic compensation for active filters," in *Proc. IEEE 15th Annu. Appl. Power Electron. Conf. Expo.*, Feb. 2000, pp. 399–405.

[8] P. Mattavelli, "A closed-loop selective harmonic compensation for active filters," *IEEE Trans. Ind. Appl.*, vol. 37, no. 1, pp. 81–89, Jan./Feb. 2001.

[9] P. Mattavelli, "Synchronous-frame harmonic control for high-performance AC power supplies," *IEEE Trans. Ind. Appl.*, vol. 37, no. 3, pp. 864–872, May/Jun. 2001.

[10] S. Fukuda and T. Yoda, "A novel current-tracking method for active filters based on a sinusoidal internal model," *IEEE Trans. Ind. Appl.*, vol. 37, no. 3, pp. 888–895, May/Jun. 2001.

[11] X. Yuan, J. Allmeling, W. Merk, and H. Stemmler, "Stationary frame generalized integrators for current control of active power filters with zero steady state error for current harmonics of concern under unbalanced and distorted operation conditions," in *Proc. Conf. Rec. IEEE-IAS Annu. Meeting*, Oct. 2000, pp. 2143–2150.

[12] X. Yuan, W. Merk, H. Stemmler, and J. Allmeling, "Stationary-frame generalized integrators for current control of active power filters with zero steady-state error for current harmonics of concern under unbalanced and distorted operating conditions," *IEEE Trans. Ind. Appl.*, vol. 38, no. 2, pp. 523–532, Mar./Apr. 2002.

[13] B. Burger and A. Engler, "Verfahren und Vorrichtung zur Bestimmung charakteristischer Gröen aus einem zeitlich periodischem signal," German Patent 199 49 997, Oct. 15, 1999.

[14] B. Burger and A. Engler, "Fast signal conditioning in single phase systems," in *Proc. Eur. Conf. Power Elect. Appl.*, 2001, pp. 1–10.

[15] R. I. Bojoi, G. Griva, M. Guerriero, F. Farina, F. Profumo, and V. Bostan, "Improved current control strategy for power conditioners using sinusoidal signal integrators in synchronous reference frame," in *Proc. IEEE 35th Annu. Power Electron. Spec. Conf.*, Jun. 2004, pp. 4623–4629.

[16] R. I. Bojoi, G. Griva, M. Guerriero, F. Farina, and F. Profumo, "Current control strategy for power conditioners using sinusoidal signal integrators in synchronous reference frame," *IEEE Trans. Power Electron.*, vol. 20, no. 6, pp. 1402–1412, Nov. 2005.

[17] P. Rodríguez, A. Luna, M. Ciobotaru, R. Teodorescu, and F. Blaabjerg, "Advanced grid synchronization system for power converters under unbalanced and distorted operating conditions," in *Proc. 32nd IEEE IECON*, Nov. 2006, pp. 5173–5178.

[18] M. Mojiri and A. R. Bakhshai, "An adaptive notch filter for frequency estimation of a periodic signal," *IEEE Trans. Autom. Control*, vol. 49, no. 2, pp. 314–318, Feb. 2004.

[19] P. A. Regalia, "An improved lattice-based adaptive IIR notch filter," *IEEE Trans. Signal Process.*, vol. 39, no. 9, pp. 2124–2128, Sep. 1991.

[20] M. Bodson and S. C. Douglas, "Adaptive algorithms for the rejection of sinusoidal disturbances with unknown frequency," *Automatica*, vol. 33, no. 12, pp. 2213–2221, Dec. 1997.

[21] L. Hsu, R. Ortega, and G. Damm, "A globally convergent frequency estimator," *IEEE Trans. Autom. Control*, vol. 44, no. 4, pp. 698–713, Apr. 1999.

[22] L. Asiminoaei, F. Blaabjerg, and S. Hansen, "Evaluation of harmonic detection methods for active power filter applications," in *Proc. IEEE 20th Annu. Appl. Power Electron. Conf. Expo.*, Mar. 2005, pp. 635–641.

[23] P. Rodríguez, A. Luna, I. Candela, R. Teodorescu, and F. Blaabjerg, "Grid synchronization of power converters using multiple second order generalized integrators," in *Proc. 34th IEEE IECON.*, Nov. 2008, pp. 755–760.

[24] P. Rodríguez, A. Luna, I. Etxeberria, J. R. Hermoso, and R. Teodorescu, "Multiple second order generalized integrators for harmonic synchronization of power converters," in *Proc. IEEE Energy Convers. Congr. Expo.*, Sep. 2009, pp. 2239–2246.

[25] P. Rodríguez, A. Luna, I. Candela, R. Mujal, R. Teodorescu, and F. Blaabjerg, "Multiresonant frequency-locked loop for grid synchronization of power converters under distorted grid conditions," *IEEE Trans. Ind. Electron.*, vol. 58, no. 1, pp. 127–138, Jan. 2011.

[26] M. Mojiri, M. Karimi-Ghartemani, and A. Bakhshai, "Time-domain signal analysis using adaptive notch filter," *IEEE Trans. Signal Process.*, vol. 55, no. 1, pp. 85–93, Jan. 2007.

[27] M. Mojiri and A. Bakhshai, "Estimation of *n* frequencies using adaptive notch filter," *IEEE Trans. Circuits Syst. II, Exp. Briefs*, vol. 54, no. 4, pp. 338–342, Apr. 2007.

[28] D. Yazdani, M. Mojiri, A. Bakhshai, and G. Joos, "A fast and accurate synchronization technique for extraction of symmetrical components," *IEEE Trans. Power Electron.*, vol. 24, no. 3, pp. 674–684, Mar. 2009.

[29] J. Matas, M. Castilla, L. G. de Vicuña, J. Miret, and J. C. Vasquez, "Virtual impedance loop for droop-controlled single-phase parallel inverters using a second-order general-integrator scheme," *IEEE Trans. Power Electron.*, vol. 25, no. 12, pp. 2993–3002, Dec. 2010.

[30] G. Wang *et al.*, "Enhanced position observer using second-order generalized integrator for sensorless interior permanent magnet synchronous motor drives," *IEEE Trans. Energy Convers.*, vol. 29, no. 2, pp. 486–495, Jun. 2014.

[31] Z. Xin, P. C. Loh, X. Wang, F. Blaabjerg, and Y. Tang, "Highly accurate derivatives for LCL-filtered grid converter with capacitor voltage active damping," *IEEE Trans. Power Electron.*, vol. 31, no. 5, pp. 3612–3625, May 2016.

[32] J. A. Suul, A. Luna, P. Rodríguez, and T. Undeland, "Virtual-flux-based voltage-sensor-less power control for unbalanced grid conditions," *IEEE Trans. Power Electron.*, vol. 27, no. 9, pp. 4071–4087, Sep. 2012.

[33] R. Wijshoff, M. Mischi, and R. Aarts, "Reduction of periodic motion artifacts in photoplethysmography," *IEEE Trans. Biomed. Eng.*, doi: 10.1109/TBME.2016.2553060.

[34] M. Ghadiri-Modarres, M. Mojiri, and M. Karimi-Ghartemani, "New adaptive algorithm for delay estimation of sinusoidal signals with unknown frequency," *IEEE Trans. Instrum. Meas.*, vol. 64, no. 9, pp. 2360–2366, Sep. 2015.

[35] M. Mansouri, M. Mojiri, M. A. Ghadiri-Modarres, and M. Karimi-Ghartemani, "Estimation of electromechanical oscillations from phasor measurements using second-order generalized integrator," *IEEE Trans. Instrum. Meas.*, vol. 64, no. 4, pp. 943–950, Apr. 2015.

[36] J. H. Allmeling, "A control structure for fast harmonics compensation in active filters," in *Proc. IEEE 33rd Annu. Power Electron. Specialists Conf.*, Jun. 2002, pp. 376–381.

[37] J. Allmeling, "A control structure for fast harmonics compensation in active filters," *IEEE Trans. Power Electron.*, vol. 19, no. 2, pp. 508–514, Mar. 2004.

[38] X. Guo, W. Wu, and Z. Chen, "Multiple-complex coefficient-filter-based phase-locked loop and synchronization technique for three-phase grid-interfaced converters in distributed utility networks," *IEEE Trans. Ind. Electron.*, vol. 58, no. 4, pp. 1194–1204, Apr. 2011.

[39] X. Zhao, X. Jin, F. Zhou, and G. Ge, "A frequency-locked loop technology of grid-connected inverters based on the reduced order resonant controller," *Proc. CSEE*, vol. 33, no. 15, pp. 38–44, May 2013.

[40] M. Ciobotaru, R. Teodorescu, and V. G. Agelidis, "Offset rejection for PLL based synchronization in grid-connected converters," in *Proc. 23rd Annu. IEEE Appl. Power Electron. Conf. Expo.*, Feb. 2008, pp. 1611–1617.

[41] M. Karimi-Ghartemani, S. A. Khajehoddin, P. K. Jain, A. Bakhshai, and M. Mojiri, "Addressing DC component in PLL and notch filter algorithms," *IEEE Trans. Power Electron.*, vol. 27, no. 1, pp. 78–86, Jan. 2012.

[42] A. J. Wang, B. Y. Ma, and C. X. Meng, "A frequency-locked loop technology of three-phase grid-connected inverter based on improved reduced order generalized integrator," in *Proc. IEEE 10th ICIEA.*, Jun. 2015, pp. 730–735.

[43] W. Li, X. Ruan, C. Bao, D. Pan, and X. Wang, "Grid synchronization systems of three-phase grid-connected power converters: A complex-vector-filter perspective," *IEEE Trans. Ind. Electron.*, vol. 61, no. 4, pp. 1855–1870, Apr. 2014.

[44] J. Matas, M. Castilla, J. Miret, L. García de Vicuña, and R. Guzman, "An adaptive prefiltering method to improve the speed/accuracy tradeoff of voltage sequence detection methods under adverse grid conditions," *IEEE Trans. Ind. Electron.*, vol. 61, no. 5, pp. 2139–2151, May 2014.

[45] Z. Xin, X. Wang, Z. Qin, M. Lu, P. C. Loh, and F. Blaabjerg, "An improved second-Order generalized integrator based quadrature signal generator," *IEEE Trans. Power Electron.*, vol. 31, no. 12, pp. 8068–8073, Dec. 2016.

[46] S. Hu, *Automatic Control Theory*, 6th ed. Beijing, China: Science Press, 2013.

[47] M. Ciobotaru, R. Teodorescu, and F. Blaabjerg, "A new single-phase PLL structure based on second order generalized integrator," in *Proc. IEEE PESC*, Jun. 2006, pp. 1–6.

[48] P. Rodríguez, A. Luna, R. S. Muñoz-Aguilar, I. Etxeberria-Otadui, R. Teodorescu, and F. Blaabjerg, "A stationary reference frame grid synchronization system for three-phase grid-connected power converters under adverse grid conditions," *IEEE Trans. Power Electron.*, vol. 27, no. 1, pp. 99–112, Jan. 2012.

[49] A. G. Yepes, F. D. Freijedo, J. Doval-Gandoy, O. López, J. Malvar, and P. Fernandez-Comesaña, "Effects of discretization methods on the performance of resonant controllers," *IEEE Trans. Power Electron.*, vol. 25, no. 7, pp. 1692–1712, Jul. 2010.

**ZHEN XIN** (S'15) was born in Shandong, China. He received the B.S. and M.S. degrees from the College of Information and Control Engineering, China University of Petroleum (Eastern China), Qingdao, China, in 2011 and 2014, respectively. He is currently pursuing the Ph.D. degree with the Department of Energy Technology, Aalborg University, Aalborg, Denmark. His current research interests include power quality, modeling and control of power converters for renewable energy systems, motor drives, and Rogowski current sensor.

**RENDE ZHAO** (M'15) was born in Shandong, China. He received the B.S. and M.S. degrees in electrical engineering from Shandong University, Jinan, China, in 1999 and 2002, respectively, and the Ph.D. degree from the College of Electrical Engineering, Zhejiang University, Hangzhou, China, in 2005. Since 2006, he has been with the China University of Petroleum (Eastern China), Qingdao, China. His research interests include renewable energy generation and motor control.

**PAOLO MATTAVELLI** (S'95–A'96–M'00–SM'10–F'15) received the master's (Hons.) and the Ph.D. degrees in electrical engineering from the University of Padua, Vicenza, Italy, in 1992 and 1995, respectively.

From 1995 to 2001, he was a Researcher with the University of Padua. From 2001 to 2005, he was an Associate Professor with the University of Udine, Udine, Italy, where he led the Power Electronics Laboratory. In 2005, he returned to the University of Padua with the same duties. From 2010 to 2012, he was a Professor with the Center for Power Electronics Systems, Bradley Department of Electrical and Computer Engineering, College of Engineering, Virginia Polytechnic Institute and State University, Blacksburg, VA, USA. Since 2015, he has been a Professor with the University of Padua, where he leads the Power Electronics Laboratory. His major fields of interest include the analysis, modeling, and analog and digital control of power converters, grid-connected converters for renewable energy systems and microgrids, and high-temperature and high-power-density power electronics. In these research fields, he has been leading several industrial and government projects.

Dr. Mattavelli served as an Associate Editor of the IEEE Transactions on Power Electronics from 2003 to 2012. He was the Industrial Power Converter Committee Technical Review Chair of the IEEE Transactions on Industry Applications from 2005 to 2010. He has been a Member-at-Large of the IEEE Power Electronics Society's Administrative Committee for terms 2003–2006, 2006–2009, and 2013–2015. He was the recipient of the Prize Paper Award from the IEEE Transactions on Power Electronics in 2005, 2006, 2011, and 2012, and the Second Prize Paper Award at the IEEE Industry Applications Annual Meeting in 2007.

**POH CHIANG LOH** received the B.Eng. (Hons.) and M.Eng. degrees from the National University of Singapore, Singapore, in 1998 and 2000, respectively, and the Ph.D. degree from Monash University, Melbourne, VIC, Australia, in 2002, all in electrical engineering. From 2013 to 2015, he was a Professor with Aalborg University, Aalborg, Denmark. Since 2015, he has been a tenured Full Professor with The Chinese University of Hong Kong. His interests are in power converters and their grid applications.

**FREDE BLAABJERG** (S'86–M'88–SM'97–F'03) received the Ph.D. degree from Aalborg University, Aalborg, Denmark, in 1922. He was with ABB-Scandia, Randers, Denmark, from 1987 to 1988. He became an Assistant Professor in 1992, an Associate Professor in 1996, and a Full Professor of power electronics and drives in 1998. His current research interests include power electronics and its applications, such as in wind turbines, photovoltaic systems, reliability, harmonics, and adjustable speed drives.

Dr. Blaabjerg has received 15 IEEE Prize Paper Awards, the IEEE PELS Distinguished Service Award in 2009, the EPE-PEMC Council Award in 2010, the IEEE William E. Newell Power Electronics Award 2014, and the Villum Kann Rasmussen Research Award 2014. He was an Editor-in-Chief of the IEEE Transactions on Power Electronics from 2006 to 2012. He has been a Distinguished Lecturer for the IEEE Power Electronics Society from 2005 to 2007 and for the IEEE Industry Applications Society from 2010 to 2011. He is nominated in 2014 by Thomson Reuters to be between the most 250 cited researchers in engineering in the world.